Influence of Tip Clearance on Unsteady Flow in Automobile Engine Pump

Jiacheng Dai[1], Jiegang Mou[1,*] and Tao Liu[1]

Abstract: The automobile engine pump is an important part of the automobile cooling system, and has a direct influence on the engine performance. Based on the SST k-ω turbulence model, unsteady numerical simulation for an automobile engine pump with different tip clearances was carried out by Fluent. To study the flow field characteristics and pressure fluctuation, the characteristics of secondary flow distribution in volute are also analyzed. The result shows that the pressure fluctuation characteristics of the flow field show obvious periodic variation at different levels of tip clearances. The peak value of pressure fluctuation at each monitoring point is dependent on the blade frequency. At the same time, with the increase of the tip clearance, the pressure fluctuation in the blade and volute is gradually increased, while the pressure fluctuation at the tip is reduced clearance. The pressure gradient in the pump also varies periodically with the rotation of the impeller. With the increase of the tip clearance, the pressure of the impeller, volute and tip clearance is gradually decreased. There are secondary flow vortexes inside the impeller, volute outlet and volute section. With the increase of tip clearance, the vortex intensity in the impeller channel is weakened, and the vortex strength at the volute outlet is intensified. On the cross section of the volute, the morphology of most vortexes has insignificant changes, but the vortex intensity decreased.

Keywords: Automobile engine pump, tip clearance, pressure fluctuation, secondary flow.

1 Introduction

The automobile engine pump is the main component of the cooling system of the automobile engine. It can increase the working pressure of the coolant in the circulation system, maintain the coolant circulation function between the relevant parts of the engine, and prevent the engine operating temperature from overheating. Therefore, its dynamic characteristics and reliability have attracted more and more attention of scholars [Hou, Jin, Liu et al. (2009); Wang, Tong, Li et al. (2012); Yong, Jiang, Yang et al. (2014)]. Furthermore, the vibration and noise in the pump are always the concern of the automobile. The pressure fluctuation of hydraulic component in the automobile pump

[1] College of Mechanical Engineering, Zhejiang University of Technology, Hangzhou, 310014, China.

[*] Corresponding Author: Jiegang Mou. Email: mjg1963@126.com.

Received: 14 March 2019; Accepted: 10 June 2019.

often leads to vibrations, which will aggravate the damage of the material and parts [Wu, Luo, Huang et al. (2000); Wang, Hu, Xu et al. (2005); Kong, Li, Li et al. (2011)].

Due to its small size, high speed, wide operating conditions and low efficiency, the internal flow field of automobile engine is more complicated. Many scholars have carried out a lot of researches about this problem. Shi et al. [Shi, Pei, Lu et al. (2013); Li, Shi, Pei et al. (2013)] had optimized the design of a diesel engine cold pump, and carried out numerical simulations of the whole flow field. It is found that the external characteristics, turbulent kinetic energy and cavitation performance of the optimized model had been improved dratically. Xue et al. [Xue, Zhang, Hou (2015); Xue (2016)] conducted a comprehensive test and analysis of vibration in different positions of an automobile pump by using the LMS eight channel vibration and noise test, which provided test data for optimal designs of the pump and how to reduce the pressure fluctuation caused by cavitation. Wu et al. [Wu, Tang, Zhang et al. (2013)] proposed a new design method for the automobile engine pump with semi-open impeller, and completed the pressure velocity coupling the dynamics model of the pump by CFD. He discovered the power of a new impeller was significantly reduced, and the efficiency was improved. Zhang et al. [Zhang, Chen, Wang et al. (2017)] studied the influence on the pressure pulsation of a screw centrifugal pump under different tip clearances, and analyzed the law of pressure pulsation in a single blade spiral centrifugal pump, which provided the reference for vibration and noise reduction of semi-open screw centrifugal pump. Shukla et al. [Shukla, Kshirsagar (2007)] carried out numerical simulations to the tip clearance of a semi-open impeller pump, and obtained the influence on the whole performance of a semi-open impeller pump under different tip clearances, proposed a flow pattern of tip clearance vortex associated with tip clearance. Kim et al. [Kim, Choi, Kim et al. (2013)] used CFD technology to carry out the design to the three different tip clearances of a turbine pump, the cavitation was found at the leading edge of the blade tip, and at high flow rate. Due to the cavitation at the pressure side of the blade and the sudden obstruction of the throat of the suction side, the head of blade burst. Through the numerical simulation method, Kim et al. [Kim, Ji, Kim (2015)] studied the influence of the tip clearance ratio and the tip clearance on the performance of the self-priming pump, and obtained the characteristic curve under different tip clearances.

So far, there are little researches on pressure fluctuation of the automotive engine pump under the tip clearance. In order to study the flow characteristics of the interior flow field of an automobile engine pump with different tip clearances, the unsteady numerical simulation for the internal flow field of the automotive engine pump was carried out for 4 tip clearance thickness dimensions, which are 0 mm, 0.3 mm, 0.5 mm, and 0.6 mm respectively, and the pressure fluctuation characteristics and transient flow field of automobile pump are also studied.

2 Investigated pump and numerical simulation methods

2.1 Computational model

The model F31D1 of automobile engine pump is taken as the object of this research. The fluid domain model is shown in Fig. 1, where the pump has two inlets with diameters of 18 mm and 30 mm and an exit with diameter of 85 mm. The pump speed n=3600 r/min, flow Q=180 L/min, head of delivery H=11.21 m, efficiency η=38.5%.

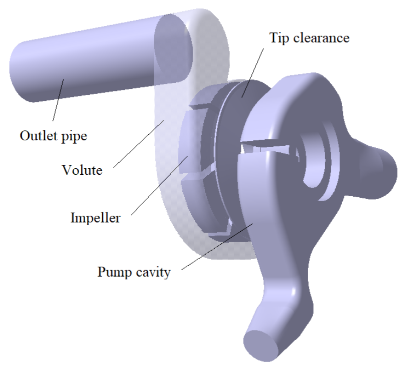

Figure 1: 3D model of fluid domain

2.2 Meshing and boundary conditions

The fluid domain of the pump consists of five parts: pump cavity, blade clearance, impeller, volute and outlet pipe. If unstructured mesh is used, it is easy to increase the surface area of the mesh and increase the computational complexity. If the structure mesh is used, it is difficult to partition the complex shape of the fluid domain, so the automobile pump adopts a hybrid tetrahedron and hexahedral unstructured mesh. The pump cavity, impeller, volute and outlet pipe are divided into unstructured meshes, and the tip clearance is divided into structural meshes. The axial direction of tip clearance, namely its thickness direction, is divided into 10 meshes, and the division of fluid domain is shown in Fig. 2, which carried out mesh independent verification by Fluent at the same time, as shown in Tab. 1. The number of mesh units was finally determined to be 1867980.

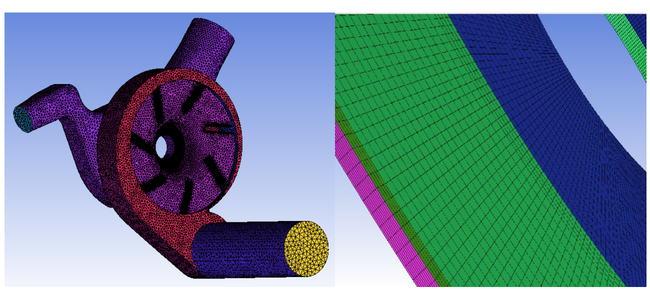

Figure 2: Mesh of fluid domain and tip clearance

Table 1: Mesh independence verification

Mesh number	Head of delivery（*m*）	Efficiency（%）
2387561	11.13	37.9
1867980	11.25	38.8
1542567	10.67	38.4
Experimental value	10.82	38.1

The pressure inlet is used to define a standard atmospheric pressure, the outlet is chosen as the outlet of the flow, and the wall is subjected to no slip condition. Using transient simulation, the time step is 0.00014 S, and the number of iterations of one time step is 20 times. The impeller rotation cycle is calculated, and the time step is set to 833 steps.

2.3 Arrangement of monitoring point

3 monitoring points are arranged on the blade pressure surface and the suction surface respectively, 5 monitoring points are arranged at the circumferential direction of the spiral case, and 3 points are arranged in the radial direction of the tip clearance, which followed by G1, G2, G3, B1, B2, B3, P0, P1, P2, P3, P4, P5, P7, S1 S2 and S3, as shown in Fig. 3.

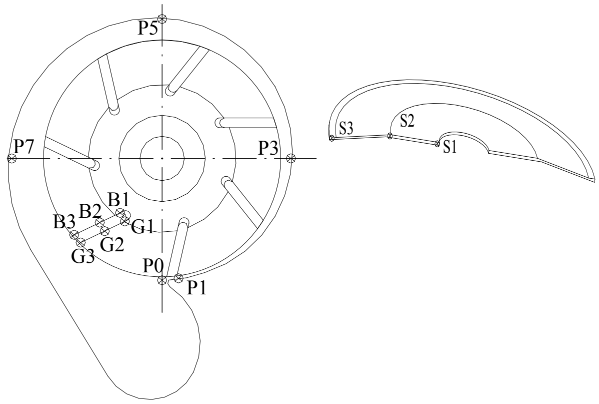

Figure 3: Location of monitoring points

2.4 Experiment analysis

The external characteristics of the automobile engine pump are tested, and the test table is shown in Fig. 4. The test table conforms to the national standard ISO 9906:2012. The simulation results compared with the experimental results are shown in Fig. 5. Compared to the original model, it can be seen from Fig. 5 that the numerical simulation results and test results are very similar, with the increase of the tip clearance, the head of delivery increases first and then decreases, and there are peak and trough in efficiency.

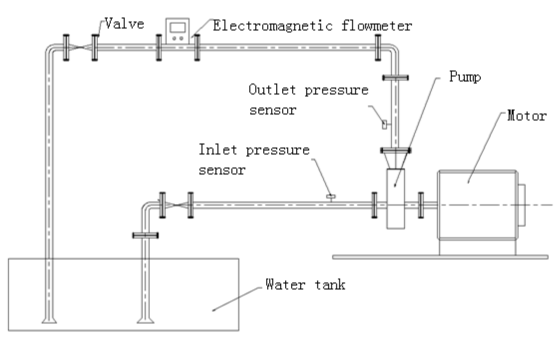

Figure 4: Pump testing table

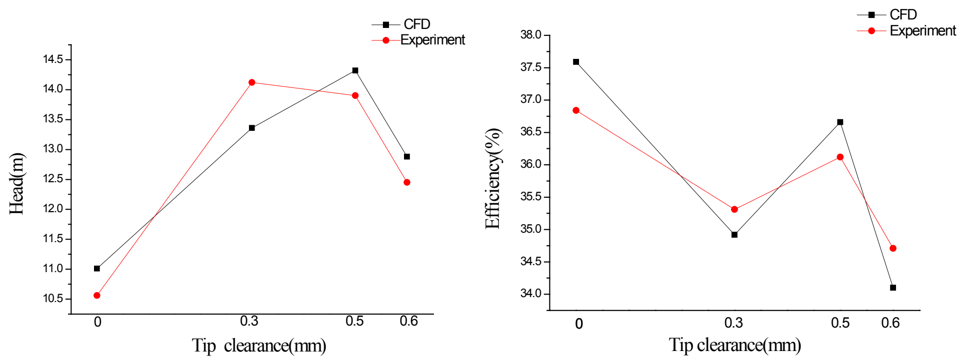

Figure 5: Test comparison

3 Pressure fluctuation analysis

The transient pressure value is treated by dimensionless method by using pressure coefficient, the formula is:

$$C_p = (p_i - \overline{p})\ /0.5\rho u_2^2 \tag{1}$$

where u2=16.041 m/s, is impeller outlet circumferential velocity, m/s; p_i is transient static pressure, pa; $\overline{p}$ is average static pressure, pa; ρ is water density, kg/m^3. These referenced in the last cycle of data for the pressure fluctuation analysis and processing.

3.1 Blade pressure fluctuation

Fig. 6 is time domain diagram of the pressure fluctuation of the monitoring points at the suction surface and the pressure surface. It can be seen from Fig. 6 that the waveforms of the pressure fluctuation vary with tip clearance and fluctuation waveform of vaneless gap have evident changes. The pressure fluctuation waveforms of the three monitoring points at the suction surface and the pressure surface are similar. Meanwhile, the fluctuation amplitude at each monitoring point is the maximum when the tip clearance is 0.6 mm, and the peak value is the largest. With the increase of the tip clearance, the pressure amplitude increases, and the peak value also increases. As the leading edge of the blade to the trailing edge, the pressure fluctuation amplitude of three monitoring points on pressure surface is gradually reduced, while the peak value remains unchanged. The pressure fluctuation amplitude of three monitoring points on the suction surface is gradually increased, and the peak value is maintained.

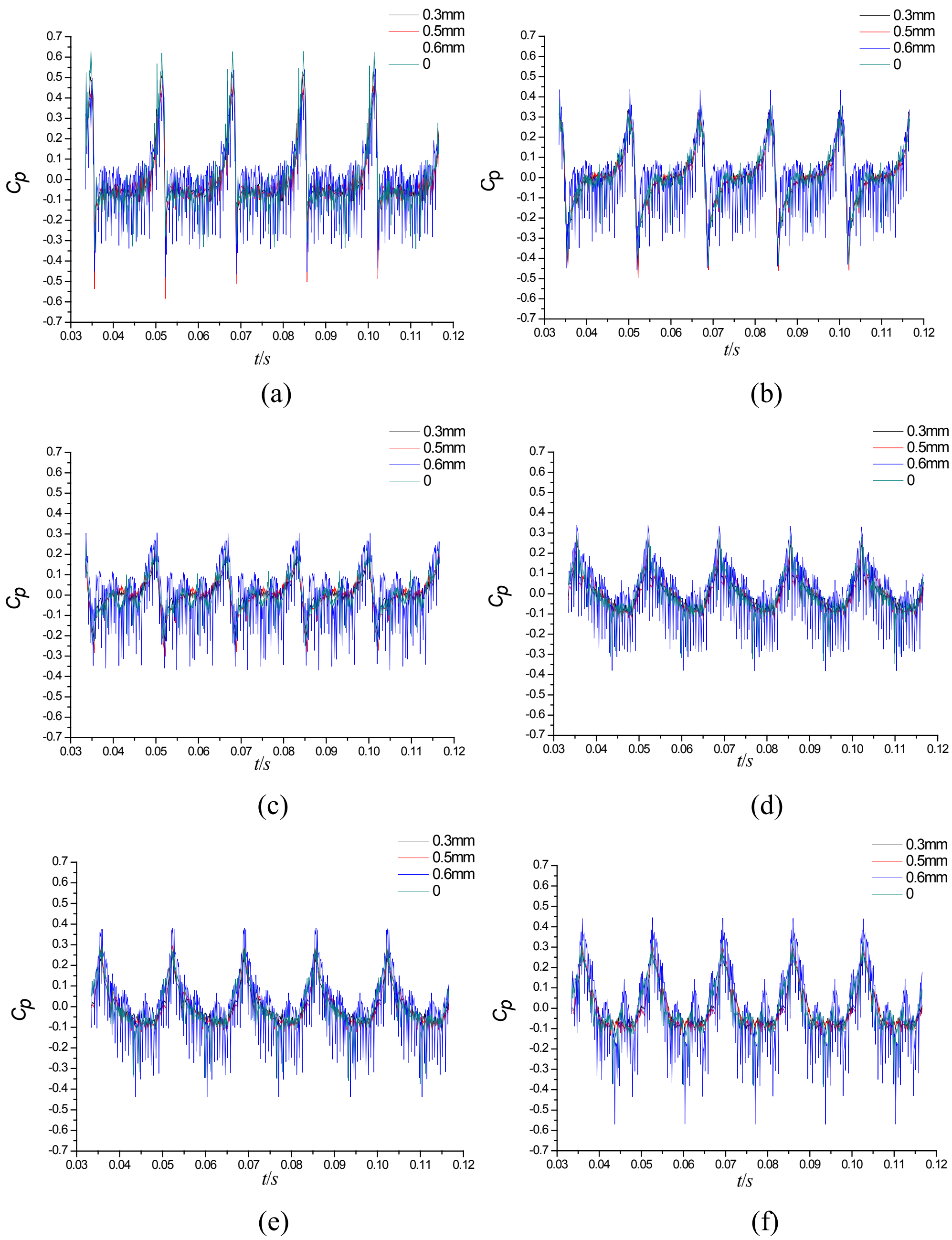

Figure 6: Time fluctuation diagram of pressure fluctuation at blade monitoring point for the (a) G1, (b) G2, (c) G3, (d) B1, (e) B2, (f) B3

3.2 Volute pressure fluctuation

Fig. 7 is time domain diagram of pressure fluctuation for monitoring points P0, P1, P3, P5, and P7. As can be seen from the graph, the pressure fluctuation of 5 monitoring points shows clear periodic variation. Since the number of blades is 7, the impeller rotates in one cycle, and the peaks and troughs appear 7 times. As found in Fig. 7, the time interval between adjacent peaks is about 0.0048 S, and the amplitude of pressure pulsation at the monitoring point P0 near the tongue is the largest because it's near the position of tongue, where the curvature change is relatively large. Each time the blade rotates through P0, it will result in a greater amount of pressure. At each monitoring point, compared with the pressure fluctuation at the monitoring point without considering the tip clearance, the pressure fluctuation at the monitoring point has obvious changes after considering the tip clearance. When tip clearance is 0.6 mm, the pressure fluctuation is significantly higher than that of the other monitoring points, and its peak value is the largest. The tip clearances for the pressure amplitude of the 0.3 mm and 0.5 mm are roughly the same, and at the same time, those waveforms are similar. With the direction of fluid flow within the volute, pressure amplitude of each monitoring points under different tip clearances are decreased. With the increase of the tip clearance, the pressure fluctuation amplitude shows a growing tendency, which shows that the decreased tip clearance can improve the pressure fluctuation of the volute.

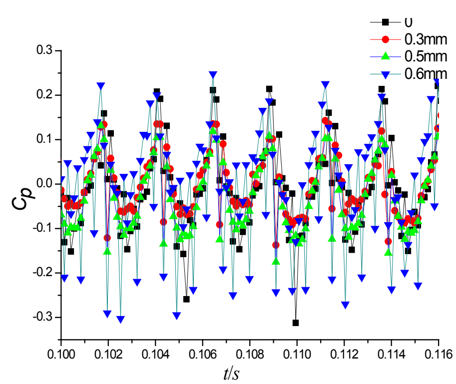

(a)

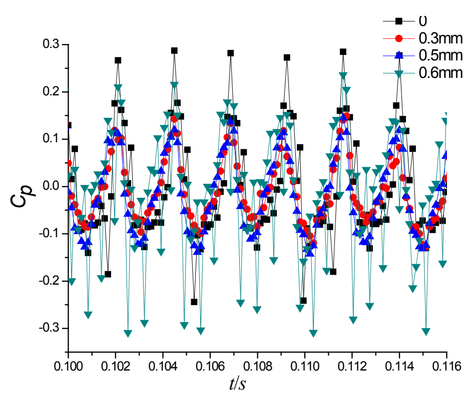

(b)

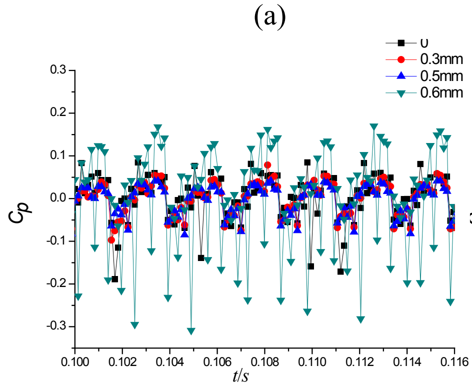

(c)

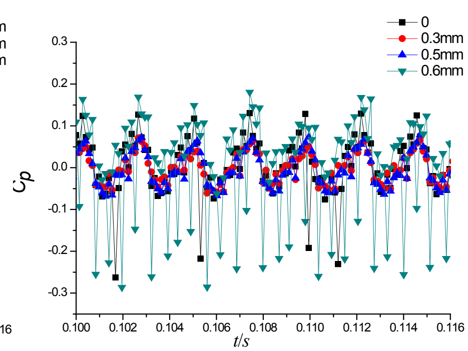

(d)

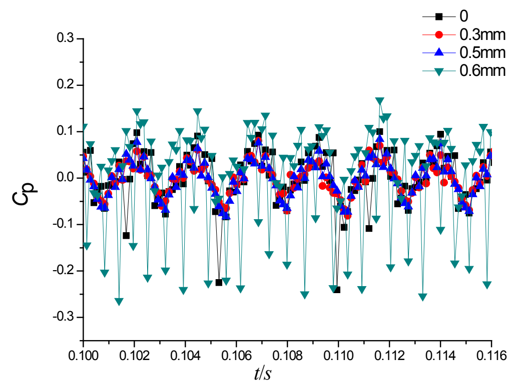

(e)

Figure 7: Time domain diagram of pressure fluctuation in spiral case monitoring points for the (a) P0, (b) P1, (c) P3, (d) P5, (e) P7

3.3 Pressure fluctuation at tip clearance

Fig. 8 is the pressure fluctuation of 3 monitoring points in radial direction of the tip clearance. It is shown that the monitoring points S1, S2 and S3 show periodical pressure fluctuation. In the monitoring points S1 and S3, the maximum amplitude of pressure fluctuation under the tip clearance of 0.6 mm is higher than that the tip clearances of 0.3 mm and 0.5 mm, and its peak value is also the largest. The fluctuation waveforms at the tip clearance of 0.3 mm and 0.5 mm remain similar. At S2 monitoring points, when the tip clearance is 0.3 mm, the pressure fluctuation amplitude is at the maximum, and the peak value is also the largest. With the increase of the tip clearance, the pressure fluctuation amplitude is decreased, and peak value is also decreased. Unlike the pressure fluctuation regularity of S1 and S3 monitoring points, since the point S2 is just at the point where the curvature of the tip clearance varies sharply, it results in a dramatic change in pressure due to a sharp change in curvature.

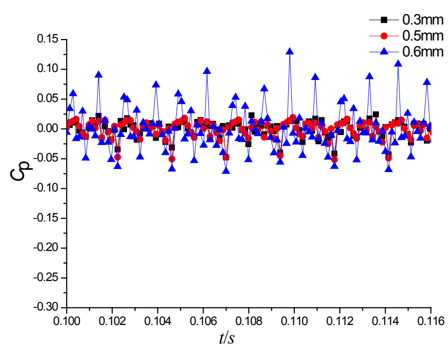

(a)

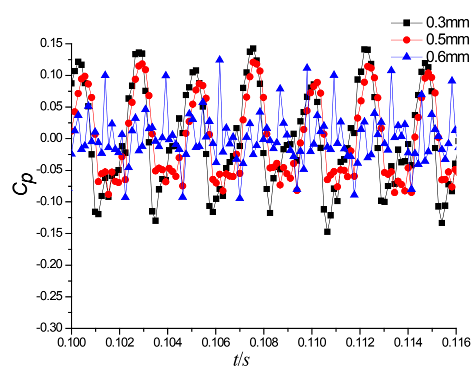

(b)

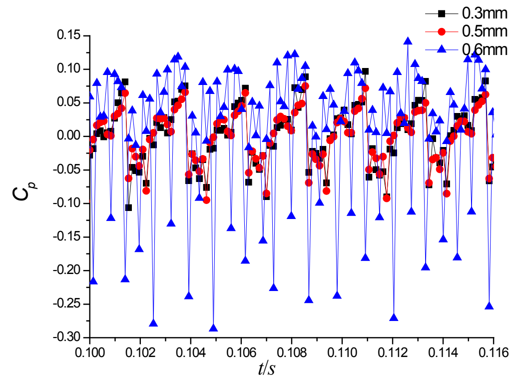

(c)

Figure 8: Time domain diagram of pressure fluctuation at monitoring point on top clearance for the (a) S1, (b) S2, (c) S3

The monitoring points P0 is regarded near the tongue, the monitoring point S2 shows that the radial curvature varies greatly with the increase of tip clearance, which is the same as the monitoring point G1 on the blade pressure surface and the B1 monitoring point on the suction surface. Besides selecting the data of the last 5 cycles to obtain the pulse frequency domain diagram by FFT, as shown in Fig. 9, the abscissa f is frequency. It can be seen from Fig. 9 that 4 monitoring points exhibit obvious pressure fluctuation frequency domain characteristics. The location monitoring points P0 near the tongue and S2 on the tip clearance show the highest values at the blade passing frequency (about 420 Hz). The monitoring points G1 near the leading edge of the blade and B1 on the suction surface show the maximum pressure fluctuation amplitude at the impeller rotating frequency (about 60 Hz). Moreover, when the rotational frequency of the impeller increases, we can see that the pressure fluctuation amplitude is gradually reduced. It can also be seen that at the position of monitoring points P0 and B1, the amplitude of pressure fluctuation without considering tip clearance is maximum. With the increase of the tip clearance, the amplitude of pressure fluctuation is decreased, and has obvious improvement. With the increase of tip clearance, the amplitude of pressure fluctuation is increased. However, the pressure fluctuation amplitude of S2 and G1 decreases obviously with the increase of tip clearance.

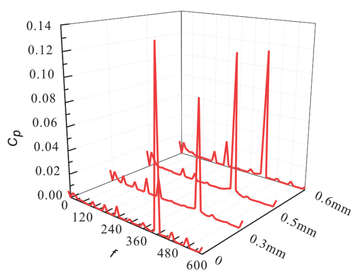

(a)

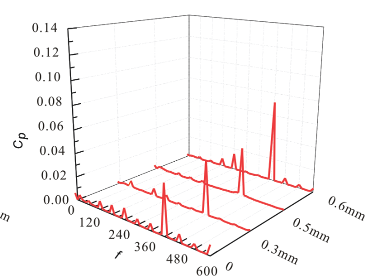

(b)

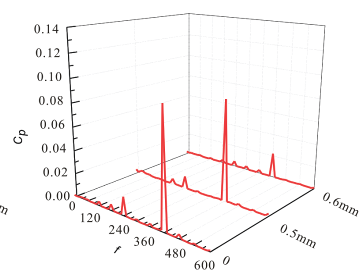

(c)

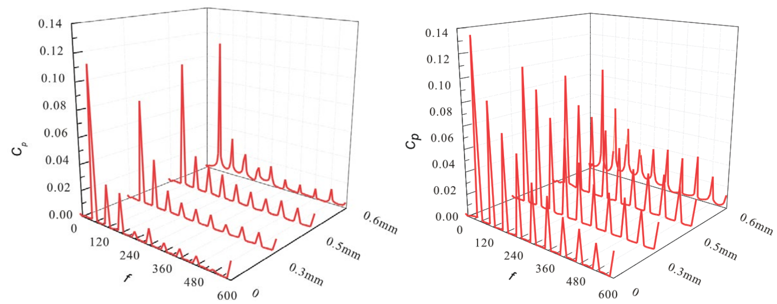

(d) (f)

Figure 9: Frequency diagram of pressure fluctuation for the (a) P0, (b) P3, (c) S2, (d) B1, (e) G1

4 Analysis of flow field

4.1 Internal flow field

Fig. 10 is the pressure distribution of middle section of impeller, which located at the middle section of the impeller. It can be seen from the chart, in the blade leading edge that the eccentric force surface has a certain area of low pressure area, while the pressure of the blade tail is higher. In one cycle, the area of low pressure area increases first and then decreases. Simultaneously, we can clearly see from the tail to the head of the blade that the pressure of blade pressure surface is always reduced, and the pressure at the back of the blade is always increased, which also illustrates the variation characteristics of blade pressure fluctuations of monitoring points. A high-pressure zone with a smaller area is formed at the pressure face of the blade leading edge near the tongue separation position. With the blade slowly sweeping across the tongue, the pressure is gradually reduced, substantially the evidence of the change. The area of the high-pressure area is also decreased, which shows that the pressure pulsation amplitude of the P0 and P1 monitoring points is large. The pressure on the volute is uniform, the pressure at the outlet is large, and the pressure does not change as the cycle changes. Meanwhile, it can be seen that the pressure decreases with the increase of the tip clearance. While the area of the low pressure area at the blade head increases clearly, and the pressure at the outlet of the volute decreases. It can be seen from Fig. 11 that there is a large area of seven star low pressure in the circle of the fluid field at the tip clearance, and there has a small area of high pressure on the encircle end face. From the time variation of t=1/4 T to t=3/4 T, the area of low pressure area is obviously increased, but the area of low pressure area decreases when the time varies from t=3/4 T to t=1.0 T. In the whole cycle, the area of the high pressure of the excircle face is steadily increased. At the same time, with the increase of tip clearance, the area of low pressure area is obviously increased, while the area of high pressure area is decreased. This shows that the pressure fluctuation amplitude of S3 above is larger.

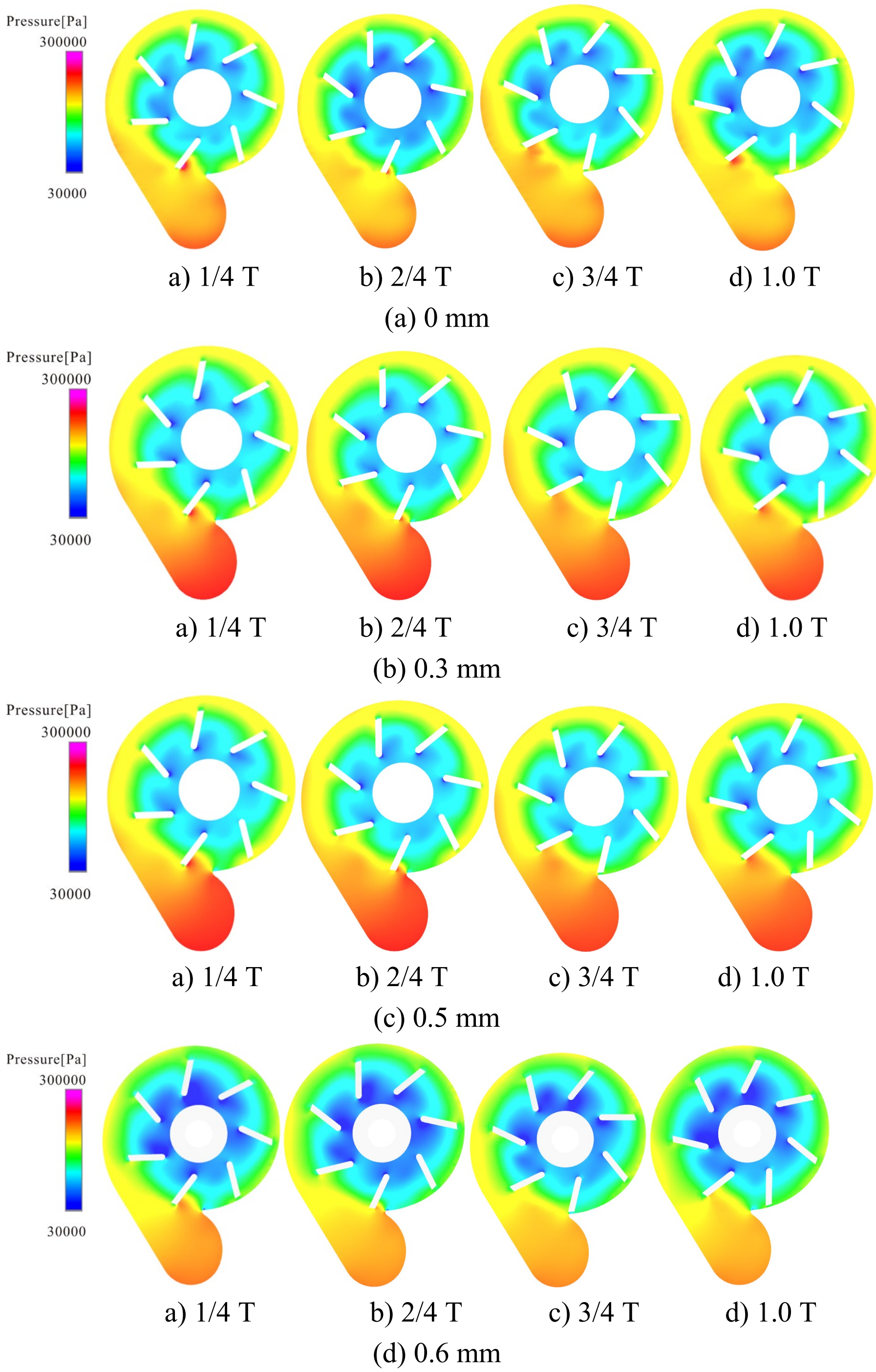

Figure 10: Pressure distribution of middle section of impeller for the (a) 0 mm, (b) 0.3 mm, (c) 0.5 mm, (d) 0.6 mm

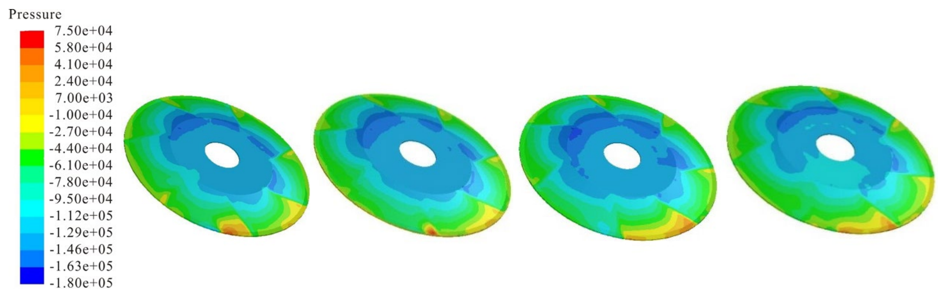

a) 1/4 T b) 2/4 T c) 3/4 T d) 1.0 T

(a) 0.3 mm

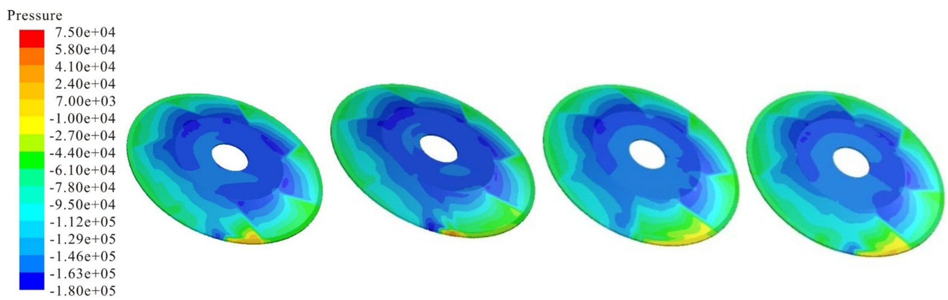

a) 1/4 T b) 2/4 T c) 3/4 T d) 1.0 T

(b) 0.5 mm

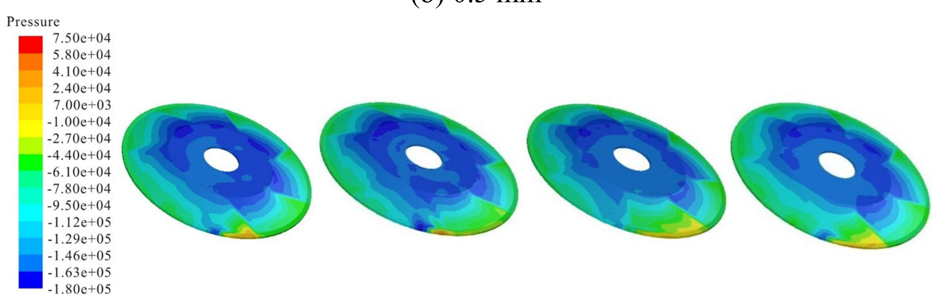

a) 1/4 T b) 2/4 T c) 3/4 T d) 1.0 T

(c) 0.6 mm

Figure 11: Pressure distribution of tip clearance for the (a) 0.3 mm, (b) 0.5 mm, (c) 0.6 mm

Fig. 12 is the velocity vector diagram of middle section of impeller. As can be seen from the chart, the fluid velocity in the blade leading edge and volute is larger, especially in the case of no-tip clearance. The flow velocity in the volute is obviously larger than that with tip clearance, while the fluid velocity at the volute exit is smaller. The fluid flow in each channel of the blade is disordered, and will create backflow vortex, especially in the position of tongue. During the journey of the volute flow, the number of vortices in the blade passage is changed from two to one, and then back to two. The flow turbulence is aggravated, and a backflow vortex is formed at the outlet of the volute. From t=1/4 T to t=1.0 T of the time change, the vortex area of the volute outlet first increase and then decrease, and the vortices in the blade passage are weakened along the direction of rotation of the impeller. Meanwhile, with the increase of tip clearance, the vortex in the blade passages is obviously weakened, while the number of vortex at the outlet of the volute becomes two, and the flow velocity is obviously reduced.

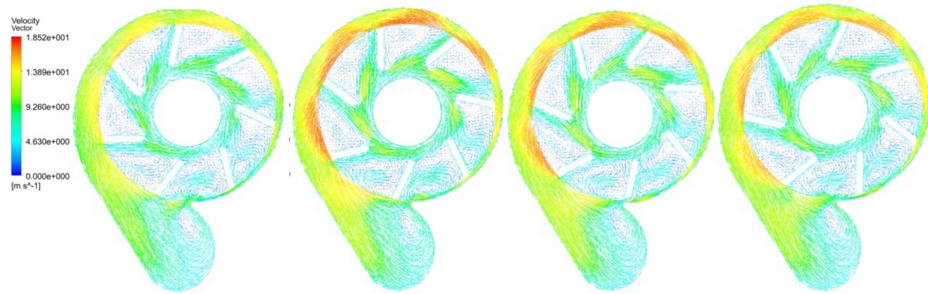

a) 1/4 T b) 2/4 T c) 3/4 T d) 1.0 T

(a) 0 mm

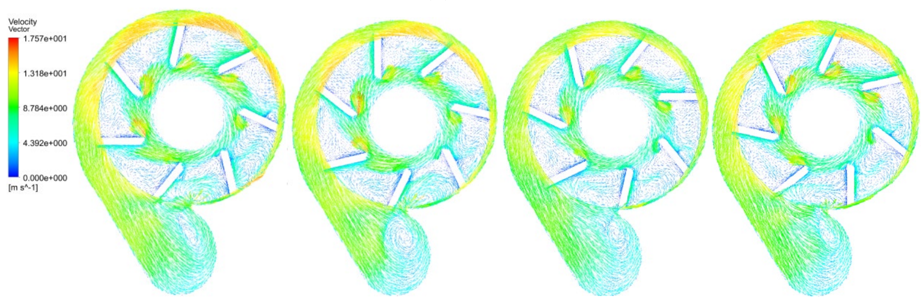

a) 1/4 T b) 2/4 T c) 3/4 T d) 1.0 T

(b) 0.3 mm

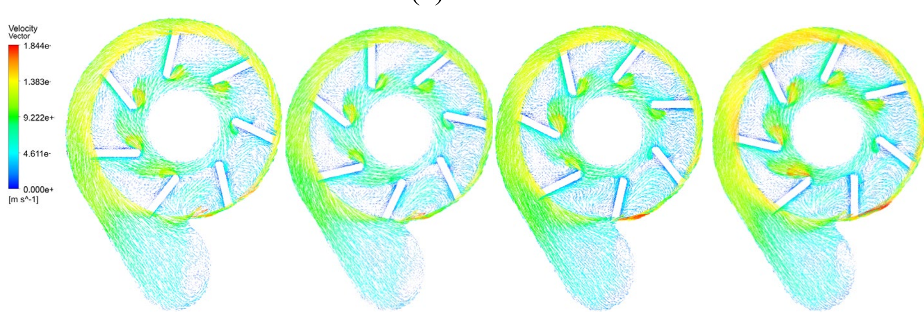

a) 1/4 T b) 2/4 T c) 3/4 T d) 1.0 T

(c) 0.5 mm

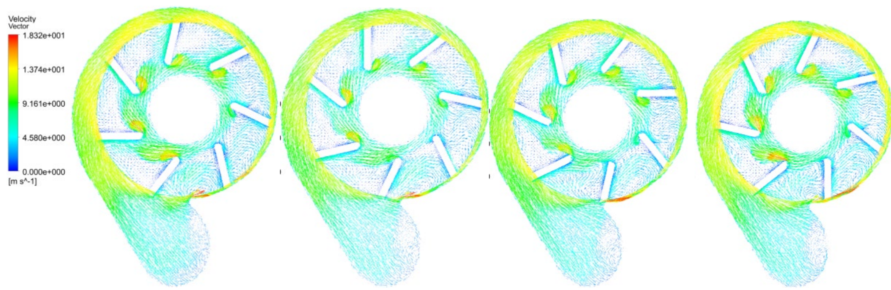

a) 1/4 T b) 2/4 T c) 3/4 T d) 1.0 T

（d）0.6 mm

Figure 12: Velocity vector diagram of middle section of impeller for the (a) 0 mm, (b) 0.3 mm, (c) 0.5 mm, (d) 0.6 mm

4.2 Secondary flow in volute

8 sections of the volute are selected to analyze the secondary flow distribution in the volute of the automobile engine pump. The sections are A, B, C, D, E, F, G and H, as shown in Fig. 13. The streamlines and vorticity are used to represent the secondary flow distribution in the 8 sections of the volute, as shown in Fig. 14. As we can see in Fig. 14, from the A section along the flow direction of the volute, the cross sectional area of the volute is obviously increased firstly. The upper and lower sides of the cross section begin to generate backflow vortices, which are asymmetrically distributed, and the area of the vortices get larger and larger. Moreover, it can be seen that the intensity of vorticity is the largest at the upper and lower ends of the cross section, and the intensity of vortices in the middle part are relatively small. A low vorticity area is formed firstly, and along the flow direction, the overall vorticity intensity decreases, whilst the area of the low vorticity in the middle part is increased. Simultaneously, with the increase of the tip clearance, vortices appear at the upper and lower ends of the cross section, and the location of the vortices center varies slightly. While the area of the vortices increases a little, the intensity of the vortices center position is obviously decreased. The area of the low vorticity in the middle part is also decreased, and the shape of vortices is simply elongated in the axial and radial directions. In particular, the vortices of eighth section change violently, and the center position of vortices moves from the left side of the section to the middle right position, then moves to the left end, while the area of the vortices increases. It can be concluded that in the design and improvement of automobile engine pump, choosing a larger tip clearance can reduce the intensity of vortices and suppress the secondary flow, which is conducive to maintain the stability of the flow field in the pump and reduce pressure fluctuation and vibration.

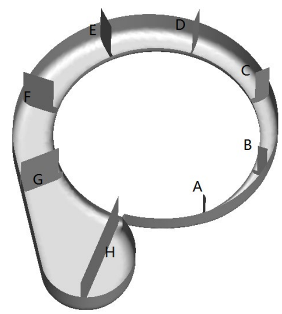

Figure 13: Cross sectional distribution of volute

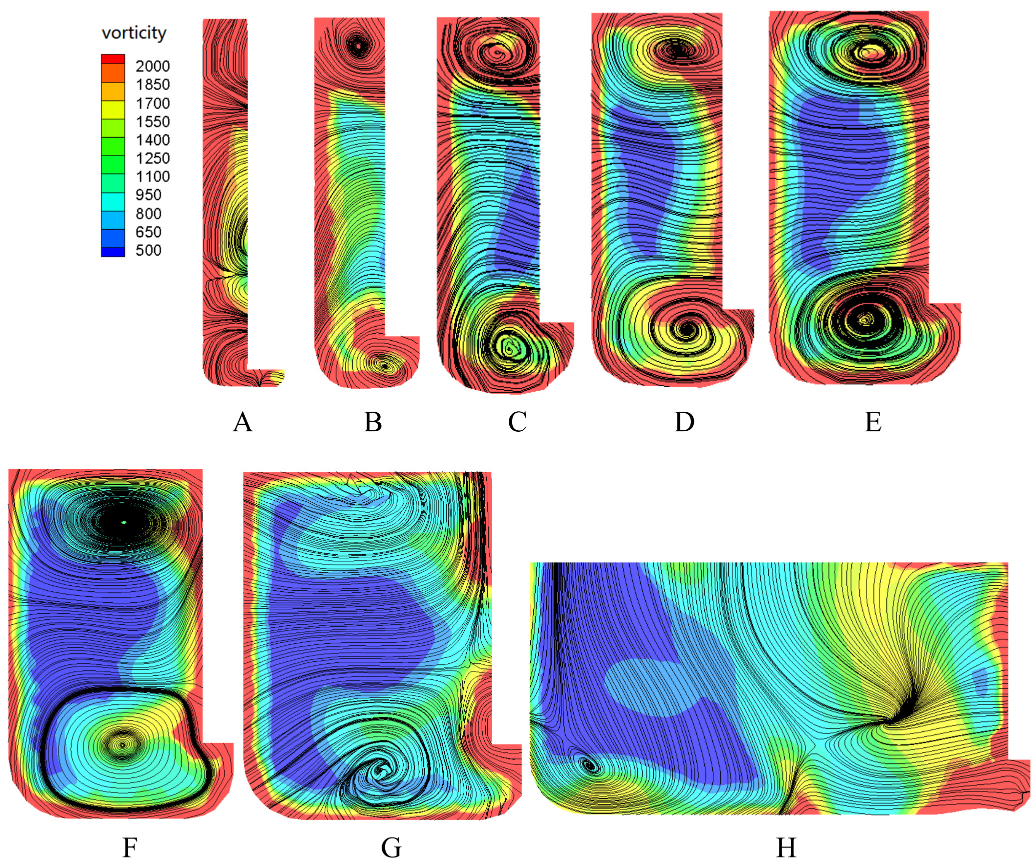

(a) 0 mm

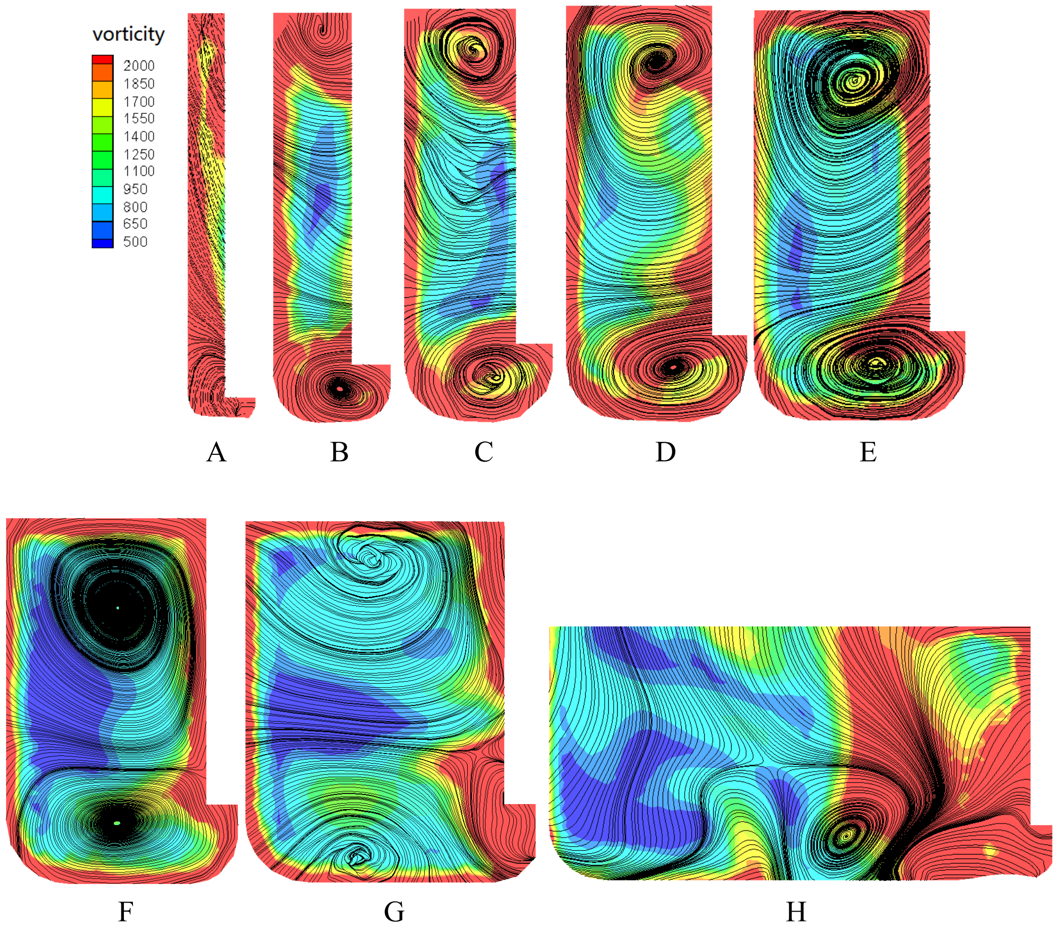
vorticity
2000
1850
1700
1550
1400
1250
1100
950
800
650
500
A
B
C
D
E
F
G
H

(b) 0.3 mm

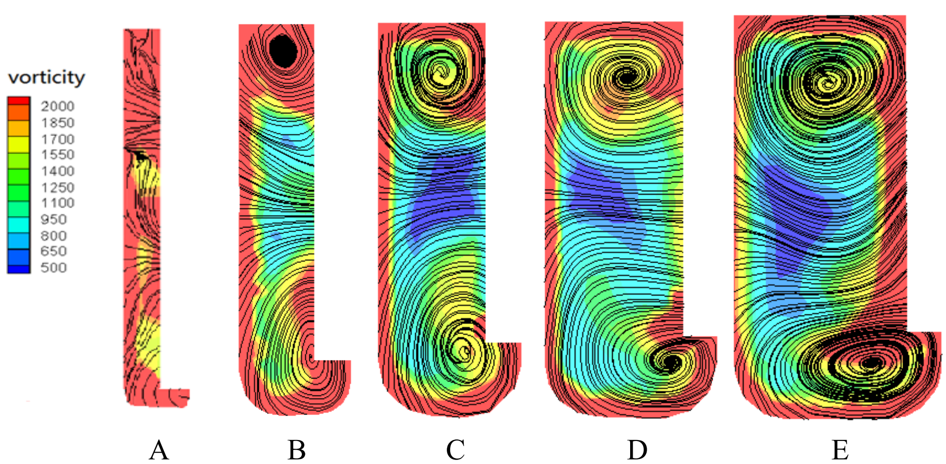
vorticity
2000
1850
1700
1550
1400
1250
1100
950
800
650
500
A
B
C
D
E

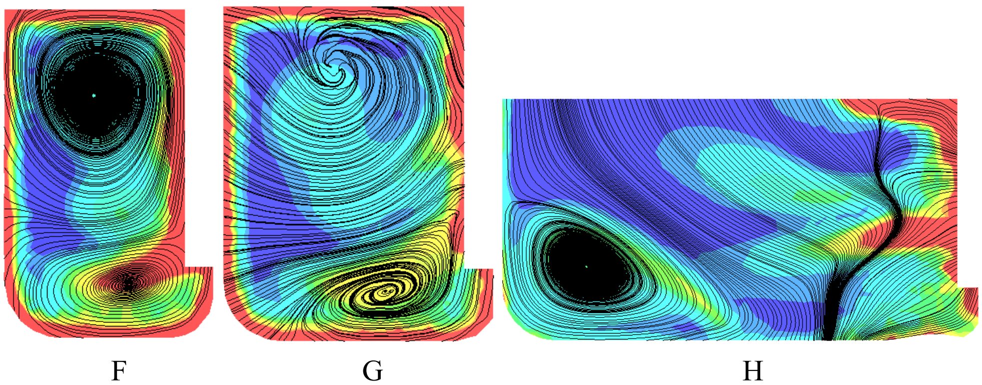

(c) 0.5 mm

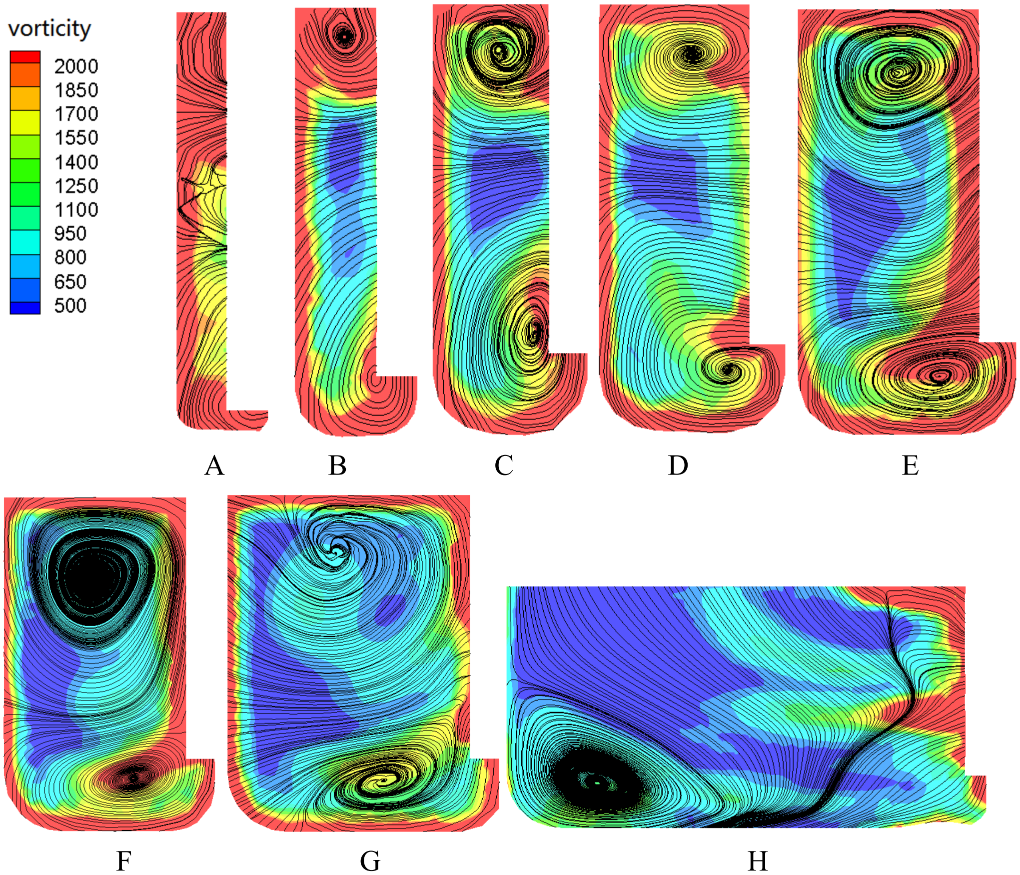

(d) 0.6 mm

Figure 14: Secondary flow of Cross section for the (a) 0 mm, (b) 0.3 mm, (c) 0.5 mm, (d) 0.6 mm

5 Conclusion

(1) The main frequency of pressure fluctuation at each monitoring point of the pump is the blade frequency. Among them, the pressure fluctuation amplitude of the monitoring points on the blade face is greater than that on suction surface. The pressure fluctuation at the monitoring point near the tongue is the strongest, and the pressure fluctuation is relatively strong where the curvature of tip clearance varies greatly. At the same time, with the increase of the tip clearance, the pressure fluctuation on the blade and volute increases gradually, while the pressure fluctuation at the tip clearance decreases.

(2) The pressure gradient in the pump varies to a great extent and varies periodically with the rotation of the impeller. The pressure on the blade leading edge is smaller, and the pressure of tongue and the outlet of volute are higher, when the pressure at the outer end of the blade clearance is the highest. Meanwhile, with the tip clearance thickness increasing, the pressure on the impeller, volute and blade gap is gradually reduced.

(3) Vortices appear in each channel of the blade and at the outlet of the volute, and change periodically. At the same time, with the top clearance thickness increasing, the flow velocity in the volute is obviously reduced, the vortex intensity in the impeller passage is weakened, and the vortex strength at the volute exit is intensified.

(4) Along the direction of fluid flow in the volute, secondary flow appears in the volute section, and changes periodically. With the increase of blade tip clearance, the shape of vortices on most sections have little change, but the strength of vortices decreases gradually.

(5) It is found that the larger tip clearance can reduce the pressure fluctuation and the intensity of the internal vortices in impeller, contributing to suppress the secondary flow and maintain the stability of the flow field in the pump. However, too large tip clearance will cause larger pressure on the blades and volute, which will induce vibration and noise. Therefore, it is necessary to select a larger tip clearance within a reasonable range. These results lay the valuable foundation for designing and modification of automobile engine pump.

Acknowledgement: The authors gratefully acknowledge the financial supports given by the National Nature Science Foundation of China (51709234).

Conflicts of Interest: The authors declare that they have no conflicts of interest to report regarding the present study.

References

Hou, X.; Jin, X.; Liu, Z.; Yan, F.; Yuan, S. (2009): Flow field analysis and improvement of automobile water pump based on fluent. *International Conference on Computational Intelligence and Software Engineering*, IEEE.

Kim, S.; Choi, C.; Kim, J.; Park, K.; Baek, J. (2013): Tip clearance effects on cavitation evolution and head breakdown in turbo pump inducer. *Journal of Propulsion & Power*, vol. 29, no. 29, pp. 1357-1366.

Kim, J. W.; Ji, H. G.; Kim, Y. J. (2015): Effect of tip clearance on the performance of self-priming vacuum pump. *Isfmfe-International Symposium on Fluid Machinery and Fluid Engineering.* IET.

Kong, W. F.; Li, L. J.; Li, P. Y.; Li, W. P. (2011): Dynamic characteristics of automobile pump assembly. *Journal of Mechanical Strength*.

Li, W.; Shi, W. D.; Pei, B.; Zhang, H.; Lu, W. G. (2013): Numerical simulation and improvement on cavitation characteristics of engine cooling water pump. *Transactions of CSICE*, vol. 2, pp. 165-170.

Shi, W. D.; Pei, B.; Lu, W. G.; Wang, C.; Li, W. (2013): Optimization of automobile pump based on CFD. *Drainage and Irrigation Machinery*, vol. 1, pp. 15-19.

Shukla, S. N.; Kshirsagar, J. (2007): Numerical simulation of tip clearance flow in semi-open impeller pump. *Asme/jsme, Joint Fluids Engineering Conference*, pp. 821-830.

Wang, H. F.; Hu, D. J.; Xu, L. M.; Ruan, Z.; Ran, L. H. (2005): Development of performance test system for oil pump in automobile engine. *Manufacturing Technology & Machine Tool*.

Wang, Z. J.; Tong, L.; Li, L. L.; Zheng, J. S. (2012): Numerical simulation of three-dimensional flow in centrifugal pump and performance prediction based on CFD. *Fluid Machinery*, vol. 40, no. 6, pp. 14-18.

Wu, J.; Tang, Q.; Zhang, Y. X.; Feng, Q. X. (2013): Impeller design and experiment for automobile water pump based on CFD. *Mechanical Research & Application*, vol. 26, no. 2, pp. 89-91.

Wu, T. F.; Luo, W. G.; Huang, J. Q.; Mo, J. W.; Zhang, H. T. (2000): The development of a computer testing system for a cooling pump of an automobile engine. *Journal of Guangxi Institute of Technology*.

Xue, D. Q.; Zhang, L. H.; Hou, S. L. (2015): Numerical simulation study on cavitation of cooling pump in mine-used vehicle based on CFD. *Mining & Processing Equipment*, vol. 2, pp. 37-41.

Xue, D. Q. (2016): Analysis on orthogonal optimization of cooling pump in agricultural vehicle based on CFD. *Journal of Chinese Agricultural Mechanization*, vol. 37, no. 9, pp. 135-139.

Yong, Y.; Jiang, W. P.; Yang, K.; Chen, X. D.; Xie, R. et al. (2014): Optimum design of automobile water pump based on CFD. *Journal of Drainage & Irrigation Machinery Engineering*, vol. 32, no. 6, pp. 477-481.

Zhang, H.; Chen, B.; Wang, B. Q.; Shi, C. B.; Shen, D. W. (2017): Influence of tip clearance on internal pressure fluctuation of screw centrifugal pump. *Transactions of the Chinese Society of Agricultural Engineering*, vol. 33, no. 1, pp. 84-89.